Time-dependent reactive scattering for the system H-+D-2 <-> HD+D- and comparison with H-+H-2 <-> H-2+H-

ARTICLE *in* THE JOURNAL OF PHYSICAL CHEMISTRY A · APRIL 2005

Impact Factor: 2.69 · DOI: 10.1021/jp0462963 · Source: PubMed

2 AUTHORS:

Cristian Morari
National Institute for Research and Develop…
40 PUBLICATIONS **201** CITATIONS
SEE PROFILE

Ralph Jaquet
Universität Siegen
63 PUBLICATIONS **1,015** CITATIONS
SEE PROFILE

Time-Dependent Reactive Scattering for the System $H^- + D_2 \leftrightarrow HD + D^-$ and Comparison with $H^- + H_2 \leftrightarrow H_2 + H^-$

Cristian Morari and Ralph Jaquet*

Theoretische Chemie, Universität Siegen, D-57068 Siegen, Germany

Received: August 17, 2004; In Final Form: December 3, 2004

This work presents results of quantum mechanical calculations of reaction probabilities for the ion−neutral molecule collisions $H^- + D_2 \leftrightarrow HD + D^-$. Time-dependent wave packet propagations for total angular momentum $J \neq 0$, including the full Coriolis coupling, are performed. The calculated state-to-state reaction probabilities using product Jacobi coordinates are compared with energy-resolved reaction probabilities calculated with the flux-operator using reactant Jacobi coordinates and with time-independent calculations. Differences between nearly converged integral cross sections and those using the *J*-shifting method and centrifugal sudden approximation and comparison with experimental results will be presented.

1. Introduction

Reactive scattering is one of the fundamental processes in atomic and molecular collision dynamics. Reactions of hydrogen systems are of a particular interest in this respect, because they are amenable to the most rigorous theoretical treatment and thus represent ideal prototype cases for a detailed comparison of theory and experiment. This is best exemplified by the neutral hydrogen system $H + H_2$ and $F + H_2$ or the ionic system $He + H_2^+$. Quantum chemistry has provided a very accurate potential energy surface (PESs) for these systems, especially for $H + H_2$. The collision dynamics are treated by quasi-classical trajectory calculations or by rigorous, fully converged quantum calculations. There are a considerable number of very detailed experimental results on which theory can be tested. A recent review summarizes the theoretical approaches.[1]

Time-dependent quantum mechanical methods have become a practical tool in studying a wide variety of molecular processes, because of their ease in implementation. To study the dynamics of elementary gas-phase reactions, such methods are used extensively, today more often than time-independent approaches. We investigate reactions of the type A + BC (A = Ne, H(D); B,C = H(D)), where one collision partner is ionic (negative or positive).[2−9] In the case of $H^- + H_2$, we use PESs available from the literature.[10,11] Our main aim is to perform time-dependent scattering calculations using wave packets, to calculate S-matrices and state-to-state reaction probabilities, and to analyze transition-state resonances. In an earlier work we presented results for the purely hydrogenic reactive system $H^- + H_2 \leftrightarrow H_2 + H^-$, and in the present work we want to concentrate on differences in reaction probabilities when the colliding diatomic molecule is replaced by the heavier isotopomer D_2. We will compare our data with the experimental crossed-beam measurements of Zimmer and Linder[12] and the guided ion beam experiments of Haufler et al.[13]

2. Wave Packet Theory

The time-dependent Schrödinger equation is solved using Jacobi coordinates by propagating wave packets with the Chebychev method (CH),[14,15] using the recursions of (a) Kosloff[14] and (b) Mandelshtam and Taylor.[16] The wave function (i.e., wave packet, (WP) is discretized on a grid,[14,17−20] so that the kinetic energy can be calculated easily within a fast Fourier transformation[21] (FFT) or discrete variable representation[22] (DVR) method. The propagation is done for a complex or real (Gray and Balint-Kurti[23]) functional form. At the end of the propagation, the wave packet is analyzed using the analysis line method.[20] The analysis can be done energy-resolved: (a) calculating state-to-state information or (b) summing reaction probabilities in the form of fluxes through an intersection surface. For the reactive investigation, we use absorbing potentials[24] in order to reduce the number of geometrical arrangements or to get rid of numerical problems at the grid edges. In oder to have all the information needed for integral cross sections, calculations are performed for different total angular momentum *J* up to $J = 60$, including the full Coriolis coupling. Within a parallel implementation, we tested different schemes for propagations, kinetic energy representations, and absorbing potentials.

2.1. Outline of the Method. The main features of our wave packet implementation are the following: We start with the *initial wave packet*,

$$\Psi(R,\mathbf{q},t=0) = \frac{1}{\sqrt[4]{\pi}\sqrt{\sigma}} \exp\left(ik_0 R - \frac{(R-R_0)^2}{2\sigma^2}\right)\chi(\mathbf{q}) \quad (1)$$

$$\chi(\mathbf{q}) = \chi_{vj}(r)\sqrt{\frac{(2j+1)}{2}\frac{(j-\Omega)!}{(j+\Omega)!}}P_j^{\Omega}(\cos\theta) \quad (2)$$

where *R* is the distance between atom A and the center of mass of the BC molecule, $\{q_i\}$ are the internal degrees of freedom for the BC molecule, and $\chi(\mathbf{q})$ is the initial state of the BC molecule for given vibrational (v) and rotational (j, Ω) quantum numbers. R_0, k_0, and σ define the initial location of the center of the wave packet in coordinate and momentum space and the initial width, respectively.

The dynamics of the system are followed by solving *the time-dependent Schrödinger equation* for nuclear motion numerically:

* Corresponding author. E-mail: ralph.jaquet@theo.chemie.uni-siegen.de.

10.1021/jp0462963 CCC: $30.25
Published on Web 00/00/0000 PAGE EST: 8.9

$$i\hbar \frac{\partial \psi(R_\alpha,r_\alpha,\theta,t)}{\partial t} = \hat{H}\psi(R_\alpha,r_\alpha,\theta,t) \quad (3)$$

α is used as an index for the different arrangements (α = A + BC, β = AB + C, γ = AC + B). The formal solution is given by

$$\Psi(t) = \hat{U}(t)\Psi(0) = \mathrm{e}^{-i\hat{H}t/\hbar}\,\Psi(0) \quad (4)$$

with $\hat{U}$ being the evolution operator for the Schrödinger equation. $\Psi(t = 0)$ and $\Psi(t)$ are the wave functions of the system at time 0 and t, respectively.

The *Hamiltonian operator* in *Jacobi coordinates* (R,r,θ) for the body-fixed frame ($\hbar = 1$) is given as

$$\hat{H} = -\frac{1}{2\mu_R}\frac{\partial^2}{\partial R^2} - \frac{1}{2\mu_r}\frac{\partial^2}{\partial r^2} - \frac{1}{2I}\left(\frac{1}{\sin\theta}\frac{\partial}{\partial\theta}\sin\theta\,\frac{\partial}{\partial\theta} - \frac{\hat{j}_z^{\,2}}{\sin\theta^2}\right) + \frac{1}{2\mu_R R^2}(\hat{J}^2 - 2\hat{J}_{\hat{z}}\hat{j}_z - \hat{J}_+\hat{j}_- - \hat{J}_-\hat{j}_+) + V(R,r,\theta), \quad \frac{1}{I} = \frac{1}{\mu_R R^2} + \frac{1}{\mu_r r^2} \quad (5)$$

μ_R is the reduced mass of the A−BC system, μ_r is the reduced mass of the BC (diatom) molecule, $\hat{J}$ is the total angular momentum operator of the system, $\hat{j}$ is the rotational angular momentum operator for BC, $V(R,r,\theta)$ is the potential energy surface, and $\hat{J}_\pm$, $\hat{j}_\pm$ are usual ladder operators for the angular momentum.

The space-fixed wave function (with Euler angles ω) for a particular total angular momentum quantum number J and its projection M on the space-fixed z-axis can be expressed in terms of body-fixed (BF) coordinates in the form

$$\Psi^{JM}(R_\alpha,r_\alpha,\theta_\alpha,\omega_\alpha,t) = \frac{1}{R_\alpha r_\alpha}\sum_{\Omega_\alpha=-J}^{J}\sqrt{\frac{2J+1}{8\pi^2}}D^J_{\Omega_\alpha,M}(\omega_\alpha)\Psi^J_{\Omega_\alpha}(R_\alpha,r_\alpha,\theta_\alpha,t) \quad (6)$$

where Ω_α is the quantum number for the projection of J (and j_α) on the body-fixed z-axis. $D^J_{\Omega_\alpha,M}$ denotes the Wigner rotation matrix elements. The resulting Hamiltonian in the body-fixed frame is given in a tridiagonal matrix representation, where, according to (5), the diagonal part is of the form

$$H_\Omega = -\frac{1}{2\mu_R}\frac{\partial^2}{\partial R^2} - \frac{1}{2\mu_r}\frac{\partial^2}{\partial r^2} - \frac{1}{2I}\left(\frac{1}{\sin\theta}\frac{\partial}{\partial\theta}\sin\theta\,\frac{\partial}{\partial\theta} - \frac{\hat{j}_z^{\,2}}{\sin\theta^2}\right) + \frac{1}{2\mu_R R^2}(\hat{J}^2 - 2\Omega^2) + V(R,r,\theta) \quad (7)$$

with the coupling term

$$H_{\Omega,\pm} = -\frac{1}{2\mu_R R^2}(\hat{J}_\pm\hat{j}_\mp) \quad (8)$$

The action of terms of type H_Ω and $H_{\Omega,\pm}$ on the wave function $\Psi^J_{\Omega_\alpha}$ (see eq 6) can be computed independently and is optimal for a parallel implementation[25] (see section 2.2). The *propagation* of the wave packet is performed using Chebyshev (CH) polynomials, originally proposed by Tal-Ezer and Kosloff.[15] We use an improved version of the Chebyshev expansion ("with one long propagation"), which was developed by Mandelshtam and Taylor.[16] It includes in the propagation the damping factor ($\mathrm{e}^{-\gamma(R,r)}$), i.e., absorbing potential (eq 11) in (R,r) space, which cancels the wave function at the end of the grid. The evolution operator (see eq 3) is expanded as (with Bessel functions J_n and Chebyshev functions Q_n)

$$\hat{U}(t) = \mathrm{e}^{-i/\hbar(\Delta E/2+V_{\min})t}\sum_{n=0}^{N}(2-\delta_{n0})(-i)^n J_n\left(\frac{\Delta E t}{2\hbar}\right)Q_n(H_s;\gamma), \quad N \approx \frac{\Delta E t}{2\hbar} \quad (9)$$

$$\mathrm{e}^{-\gamma(R,r)}Q_{n-1} + \mathrm{e}^{\gamma(R,r)}Q_{n+1} - 2H_sQ_n = 0, \quad Q_0 = 1,\ Q_1 = \mathrm{e}^{-\gamma(R,r)}H_s \quad (10)$$

$$\mathrm{e}^{-\gamma(R,r)} = \mathrm{e}^{-A_R(R-R_l)^2 - A_r(r-r_l)^2)} \quad (11)$$

H_s is a scaled and shifted Hamiltonian operator[23] (with $\Delta E = E_{\max} - E_{\min}$),

$$H_s = a_s\hat{H} + b_s, \quad a_s = \frac{2}{\Delta E},\ b_s = 1 - a_sE_{\max} \quad (12)$$

The recursion relation for the Chebyshev functions Q_n (eq 10) can be used to create the complex wave function for a given time t (see also factor N in eq 9) or used as a dynamical iteration alone.[23] In each iteration step, information needed for the final analysis will be stored.

We can perform energy-resolved state-to-state and flux calculations. The wave packet is propagated until it has "completely" left the interaction region. For the analysis, the wave packet needs to be in the correct Jacobi coordinates, depending on the different possible arrangement channels α. A basic difficulty in the theory of reactive collisions is that the coordinates appropriate for reactant and product arrangements differ from each other. There have been different ways presented in the literature to solve the problem;[26−30] one natural way would be to transform the wave function to the appropriate coordinates. This approach is time-consuming and leads to numerical errors.

Alternatively, we perform for each reactive product arrangement channel an individual scattering calculation in the appropriate product Jacobi coordinates. In case that global reaction probabilities are needed, one can calculate within the reactant Jacobi coordinates the state-to-state inelastic transition probabilities and then calculate the reaction probabilities as the difference from unity.

One disadvantage of propagation in product coordinates is that the representation of the starting wave packet needs more angular grid points for an appropriate description with a given quality of the norm of the wave function. In the present work, we calculate contributions of the wave packets at an asymptotic analysis line as proposed by Balint-Kurti et al.[20] The procedure works in the following way: in the asymptotic region, i.e., R is large, first the wave packet along a cut (R_{ana}) is projected onto the final (F) product state $\chi_F(r)$ to produce a set of time-dependent coefficients $C_{F,I}(t)$ (e.g., using product Jacobi coordinates):

$$C_{F,I}(t) = \int \mathrm{d}r\,\mathrm{d}\theta\chi^*_F(r)\Psi(R = R_{\mathrm{ana}},r,\theta,t;\mathrm{I}) \quad (13)$$

These coefficients are Fourier transformed over time to give energy-dependent coefficients $A_{F,I}(E)$:

$$A_{F,I}(E) = \frac{1}{2\pi}\int_0^\infty \mathrm{e}^{iEt/\hbar}C_{F,I}(t) \quad (14)$$

and the S-matrix results from

$$S_{F,I}^{\alpha',\alpha}(E) = -\left(\frac{\hbar^2 k_F^{\alpha'} k_I^{\alpha}}{\mu^{\alpha'}\mu^{\alpha}}\right)^{1/2} e^{-ik_F^{\alpha'}R_\infty} \frac{A_{F,I}(E)}{a_E(-k_I^{\alpha})} \quad (15)$$

For energy-resolved reaction probabilities $P_{v,j}^{RE}(E)$ (e.g., using reactant Jacobi coordinates), we use

$$P_{v,j}^{RE}(E) = \frac{\hbar}{\mu} \mathrm{Im}\left[\left\langle \Psi(R,r_{ana},\theta,E) \middle| \frac{\partial \Psi(R,r_{ana},\theta,E)}{\partial r} \right\rangle\right] \quad (16)$$

$$P_{v,j}^{IN}(E) = \frac{\hbar}{\mu} \mathrm{Im}\left[\left\langle \Psi(R_{ana},r,\theta,E) \middle| \frac{\partial \Psi(R_{ana},r,\theta,E)}{\partial r} \right\rangle\right] \quad (17)$$

In the case of reactant Jacobi coordinates, the quantity in the brackets is the energy-resolved flux of the wave packet at the asymptotic dividing surfaces defined at the position r_{ana} (for reactive (RE) analysis) or at R_{ana} (for inelastic (IN) analysis); the angular brackets denote integration over the other two coordinates. The energy-dependent wave function $\Psi(R,r,\theta,E)$ is obtained by Fourier-transforming $\Psi(R,r,\theta,t)$. Further details are given in refs 2, 23, and 31. Unphysical reflections of the wave function are minimized by a surrounding optical (absorbing) potential of the form proposed by Vibok and Balint-Kurti;[24] we mostly use the type given in eq 11.

The main features of our state selective analysis are the following:

(1) For inelastic 3D investigations, we use reactant Jacobi coordinates so that a state-to-state inelastic analysis is possible and energy-resolved total reaction probabilities can be calculated.

(2) In case of reactive 3D investigations, we use product Jacobi coordinates so that state-to-state reaction probabilities can be calculated.

2.2. Parallel Architecture. For the parallel code we exploit the structure of the Hamiltonian with respect to different projections (Ω) of the total angular momentum (J). A similar strategy had been described by Goldfield and Gray.[25] In a symmetry-adapted BF angular momentum basis, we can perform the calculations for a given total angular momentum J and parity ϵ, for either a $J+1$ or a J manifold of Ω states, depending on whether the total parity is even ($\Omega \geq 0$) or odd ($\Omega > 0$). The matrix representation of the Hamiltonian for even parity is the following:

$$H = \begin{pmatrix} H_{\Omega=0} & H_{\Omega=0,+} & 0 & 0 & 0 & \ldots \\ H_{\Omega=1,-} & H_{\Omega=1} & H_{\Omega=1,+} & 0 & 0 & \ldots \\ 0 & H_{\Omega=2,-} & H_{\Omega=2} & H_{\Omega=2,+} & 0 & \ldots \\ 0 & 0 & \ldots & \ldots & \ldots & \ldots \end{pmatrix} \quad (18)$$

where the individual contributions are given by eqs 7 and 8. Since the action of terms of type H_Ω and $H_{\Omega,\pm}$ on the wave function is computed independently, and the second part is less time-consuming than the first, the parallelization concerns just the "Ω diagonal Hamiltonian". The action of each block H_Ω on the wave function can be computed independently on different processors. The code had been tested within MPI-BLACS on an IBM-SP2[4] and recently on a new AMD-64-Opteron Cluster.

3. Results and Discussion

3.1. General Aspects. Within our project we concentrated on the reactions

(a) $H^- + H_2 \leftrightarrow H_2 + H^-$ (reactive)

(b) $H^- + D_2 \leftrightarrow D^- + HD$

(c) $D^- + H_2 \leftrightarrow H^- + HD$

where the present work is related to reaction (b), and J-dependent total reaction probabilities are compared between reactions (a) and (b). In the negative ion hydrogen system $H^- + D_2$, there are different competing processes at low energies:

$$\begin{aligned} H^- + D_2 &\leftrightarrow H^- + D_2 \quad \text{(elastic and inelastic)} \\ &\leftrightarrow HD + D^- \quad \text{(reactive)} \\ &\leftrightarrow H + D_2 + e^- \\ &\leftrightarrow HD + D + e^- \end{aligned}$$

where the present interest concerns the first two steps. This system is of great importance in hydrogen plasmas.[12] We are using the ab initio potential energy surface of Stärck and Meyer (SM);[10] in an earlier work we compared the scattering results with those ones obtained with the empirical DIM potential of Belyaev.[11] The scattering results at low energies using DIM deviate strongly from experiment and theoretical data produced with the ab initio SM potential. Nonetheless, today reactive dynamics on coupled surfaces is often performed with DIM surfaces. Reactive collinear two-state time-dependent investigations using DIM for H_3^- had been investigated by Aguillon et al.[32] In the case of inelastic investigations for H_3^- at high energies (up to kiloelectronvolts), the DIM results were reasonable compared to experiment.[33]

In an earlier work,[2] we started with calculations using a single potential energy surface, although it is likely that at higher energies ($E > 1.2$ eV) excited electronic states of H_3^- (i.e., $H_3 + e^-$) might influence the ground-state reaction. The above reactions (a)−(c) belong to the family of hydrogen exchange reactions. In contrast to the neutral reaction $H + H_2 \leftrightarrow H_2 + H$, the reaction $H^- + H_2 \leftrightarrow H_2 + H^-$ has a shallow potential well in the entrance channel ($E_{min}^{SM} = -0.0476$ eV), but the reaction barrier in the interaction region is of comparable magnitude. What distinguishes ionic systems from neutral systems is that, because of the long-range inductive interaction potential ($V \sim -1/R^4$), the important range of the PES is much more extended (at least for our systems: R(atom−diatom) > $R_{max} = 16a_0$) than in the case of neutral systems. An overview of experimental and theoretical research was given in a former work.[2] In recent work, Panda and Sathyamurthy[38] have investigated a new PES of H_3^- and performed time-dependent calculations for $J \neq 0$ similar to the work of Mahapatra and Sathymurthy.[34,35]

We compare our results with the guided ion beam experiments of Haufler et al.[13] and the crossed-beam experiments of Zimmer and Linder.[12] Both groups report integral and differential cross sections for different isotope variants. At total energies below the dissociation limit of the hydrogen molecule, the outcome of the $H^- + H_2$ collision can be inelastic excitation, rearrangement, and electron detachment, without or including rearrangement. From the analysis of the potential energy surfaces, one knows that the electron detachment channel opens up at an energy of 1.2 eV.

Because of the existence of several electronic excited states at energies $E > 1.2$ eV, nuclear dynamics calculations for those

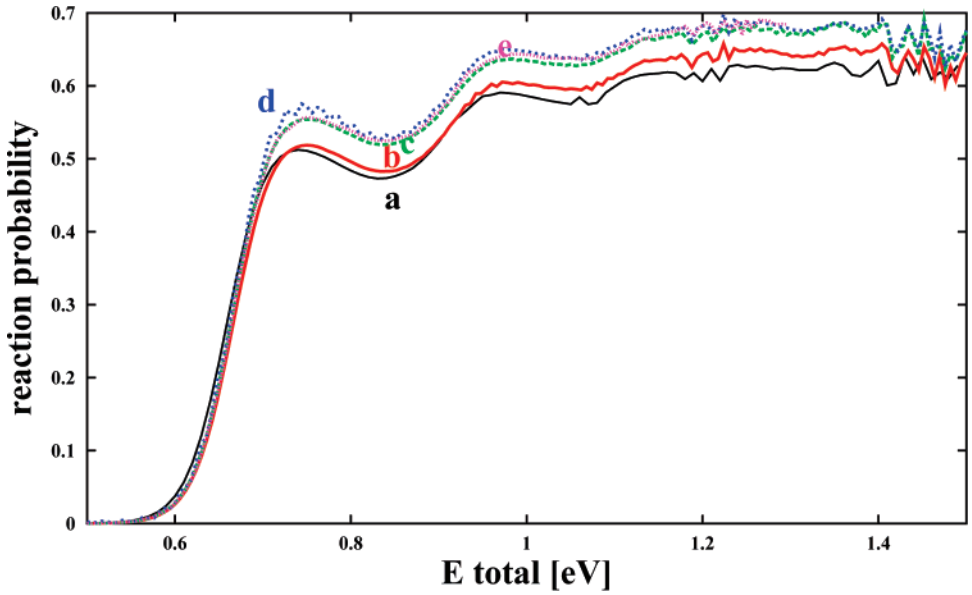

Figure 1. $H^- + D_2(v = 0, j = 0)$, total energy range $E_{total} = 0.5-1.5$ eV. Total reaction probabilities ($J = 0$) using real and complex wave packets (with different starting conditions using product (PC) or reactant coordinates (RC)) and comparison with a time-independent approach ("abc"). (a) Present code calculating state-specific (S) probabilities in the reactant region (RC) and flux (F) in the product region. (b) "Real wavepacket" code of Gray[42] using product coordinates (PC). (a,b) $R_{max} = 15.5a_0$; $E^{WP}_{trans} = 1.0$ eV. (c) Present code with $R_{max} = 17.5a_0$, in PC. (d) As in (c), but with $E^{WP}_{trans} = 2.0$ eV. (e) "abc" code:[37] scattering energy increment $\Delta E = 0.005$ eV, maximum internal energy in any channel $E_{max} = 2.5$ eV.

energies should take this into account. In this paper we present calculations on a single surface, which are reasonable at least up to $E = 1.2$ eV. The influence of higher excited states on the dynamics has to be investigated in the future. To check our code and to compare with time-independent approaches, we performed in addition calculations ($J = 0$) using the hyperspherical coordinate method of Manolopoulos et al.[37]

The numerical grid parameters and properties of the initial wave function used in the calculations of total and state-to-state reaction probabilities are similar to Table 1 given in ref 2: $(R,r,\theta)_{RC} = (128,64,32)$ and $(R,r,\theta)_{PC} = (128,128,80)$; absorbing potential (see eq 11), $A_R = A_r = 0.015$, $R(r)_I = R(r)_{max} - 4.0a_0$; analysis (see eqs 16 and 17), $R(r)_{ana} \leq R(r)_I$.

3.2. $H^- + D_2$. The present calculations have been performed for a single surface (lowest electronic state). The code used was developed by ourselves and is based on the relations described in the theory section (section 2). In a few exemplary cases, we checked the results using two other time-dependent[42] and time-independent[37] codes (tested for $J = 0$).

Investigations of the reaction dynamics for $H^- + D_2 \rightarrow HD + D^-$ featuring energy-resolved state-to-state and total reaction probabilities (differential cross sections will be presented in a future work) will give us an understanding of the dynamical behavior at the fundamental microscopic level. A comparison with experiment guides us in how far the SM potential energy surface is appropriate.

In the reaction with the rovibrational ground state of D_2 ($H^- + D_2(v = 0, j = 0)$) for $J = 0$ (Figure 1), the reaction probability P_{reac} looks similar to earlier results for $H^- + H_2(v = 0, j = 0)$[2]. A steep increase at ~0.55 eV up to 0.7 eV with magnitude of ~55% follows a slow increase up to 1.4 eV with a maximum value of ~70%. In this example, we compared our data with the real wave packet approach of Gray and Balint-Kurti and tested our implementation with Gray's code[42] (for $J = 0$). For exactly the same parameters (i.e., initial collision energy, all grid parameters, parameters for the absorption potential), we obtained nearly identical results. The differences (Figure 1) in the height of P_{reac} are attributed to the following observations: if the grid range is too small (R_{max}(atom−diatom) ≈ $15.5a_0$), the results deviate slightly from values for the grid range up to $R_{max} \approx 17.5a_0$. The starting location of the wave packet is then at a too short distance, because the long-range inductive interaction of the potential is still not leveled off. Increasing the average kinetic energy E^{WP}_{trans} in the starting wave packet (see eq 1, $E^{WP}_{trans} \sim k_0^2$) leads to a more pronounced oscillatory structure in the reaction probability at lower energies ($E_{total} \approx$ 0.7 eV) but produces numerically more reliable results at larger total energy (see discussion related to Figure 2). Furthermore, we compared our results with those obtained with the time-independent approach of Manolopoulos and co-workers[37] (using the "abc" code ($J = 0$) in hyperspherical coordinates). The maximum hyperspherical radius was set to ~$15.5a_0$ and produced the same results as time-dependent calculations with $R_{max} \approx 17.5a_0$.

Reaction probabilities (P_{reac}) for higher total energies (up to $E = 6$ eV) are presented in Figure 2: for starting wave packets with too low average kinetic energy (i.e., $E^{WP}_{trans} < 0.5$ eV), the results deviate strongly from the correct form. If one starts with $E^{WP}_{trans} \approx 0.7-1.0$ eV, the reaction probabilities seem to be numerically correct for energies $E < 3$ eV, but with $E^{WP}_{trans} \approx 2$ eV, the overall correct form of P_{reac} is given up to the dissociation limit ($E_{diss}(H_2) \approx 4.75$ eV). We can compare our P^{WP}_{reac} with time-independent calculations and see in addition the wrong behavior in the increase of P_{reac} around 5 eV: here, the internal basis set is not appropriate to describe free motion of three atoms beyond the dissociation limit. The kinky curve behavior in the "abc" results comes from the fact that, for CPU reasons, we limited ourselves to an energy grid of 0.1 eV (these calculations were done only to support our time-dependent calculations). Within one run for $E^{WP}_{trans} \approx 2.0$ eV, one can calculate P_{reac} (with a few oscillations, resulting from numerical difficulties) from $E = 0.5$ to 4.7 eV. The small oscillations can be smoothed out to get an overall impression of the energy dependence of P_{reac}; the search for physical resonances is then not possible.

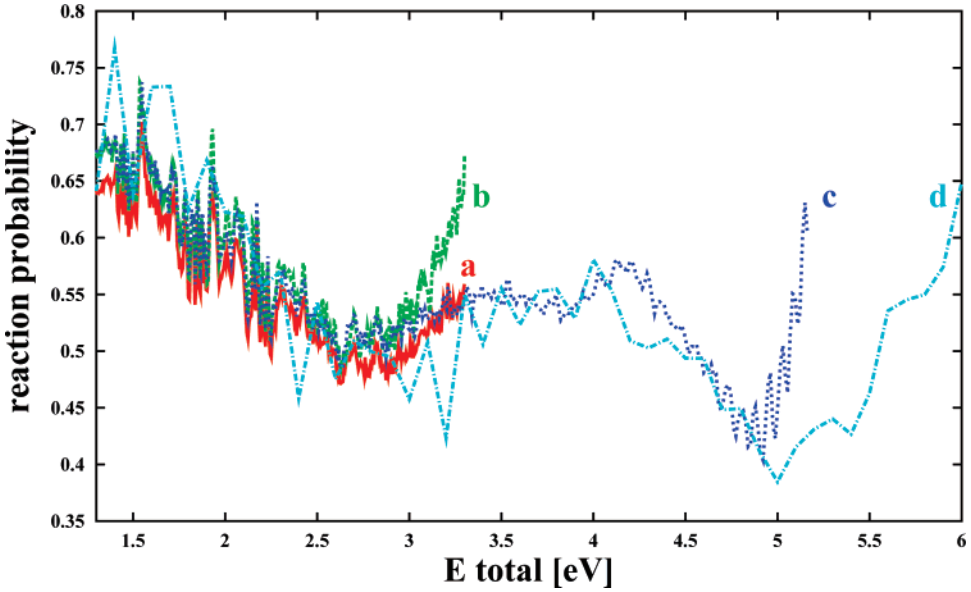

Figure 2. $H^- + D_2(v = 0, j = 0)$, total energy range $E_{total} = 1.4-6.0$ eV. Total reaction probabilities ($J = 0$). (a) "Real wavepacket" code of Gray[42] using product coordinates (PC) with $R_{max} = 15.5a_0$ and $E_{trans}^{WP} = 1.0$ eV. (b) Present code (PC, $R_{max} = 17.5a_0$, $E_{trans}^{WP} = 1.0$ eV). (c) As in (b), but with $E_{trans}^{WP} = 2.0$ eV. (d) "abc" code:[37] scattering energy increment $\Delta E = 0.1$ eV, maximum internal energy in any channel $E_{max} = 5.0$ eV.

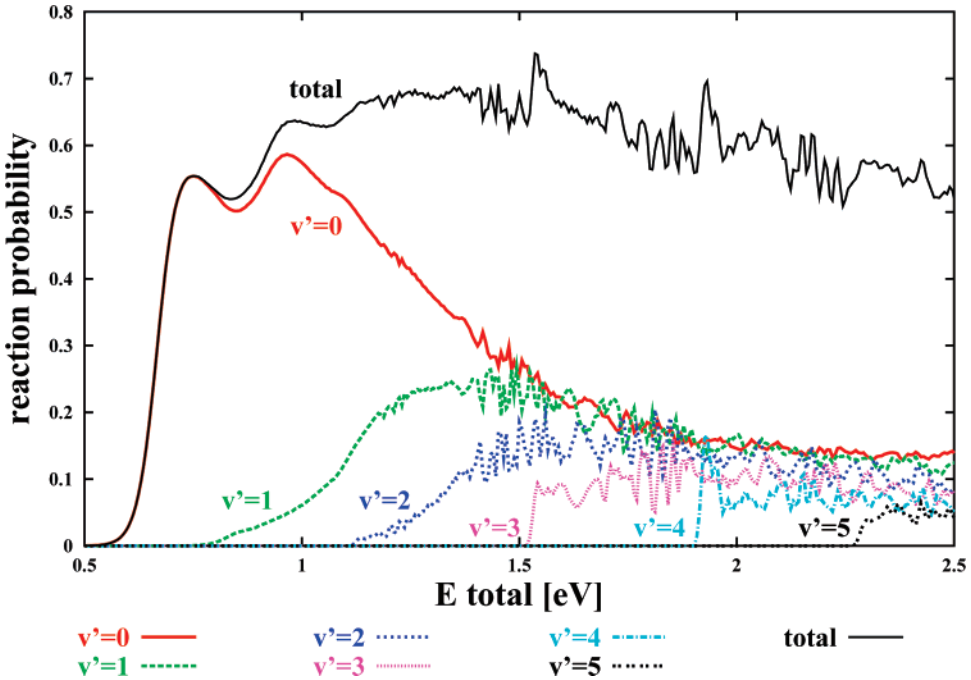

Figure 3. $H^- + D_2(v = 0, j = 0) \rightarrow HD^-(v', \Sigma j') + D$. State-to-state reaction probabilities (summed over rotational states) using product coordinates (PC) ($J = 0$; $R_{max} = 17.5a_0$, $E_{trans}^{WP} = 1$ eV).

Figure 3 presents results for state-selected reactions $H^- + D_2(v = 0, j = 0) \rightarrow D^- + HD(v', \Sigma j')$, where state-to-state reaction probabilities (summed over rotational states) using product coordinates (PC) ($J = 0$) are given. For other initial conditions ($v = 1$, 2, 3 and $j = 0$), similar results are given in Figures 4−6. All these calculations are performed for $J = 0$, $R_{max} = 17.5a_0$, and $E_{trans}^{WP} = 1$ eV.

If D_2 starts with $v = 0$, the largest reaction probability is found for HD in the final vibrational state $v' = 0$. The other vibrational states become populated when the probability of making $v' = 0$ is decreasing and leveling off (starting at $E \approx 1.5$ eV). In case of $D_2(v = 1)$, HD is produced at lower energies ($E < 0.8$ eV) with $v' = 0$, but at higher energies ($E = 0.8-1.2$ eV) $v' = 1$ is strongly favored, and for even higher energies ($E > 1.2$ eV), again $v' = 0$ predominates. If D_2 starts with $v = 2$ or $v = 3$, the final HD vibrational state is favored by $v' = v - 1$ at lower energies. For all different vibrational starting conditions and higher total energies ($E = 1.5-2.5$ eV), the vibrational ground state of the product HD($v' = 0$) is slightly dominating. For $D_2(v = 2$ or $v = 3)$, accurate reaction probabilities near the threshold are difficult to get and lead to a sharp, numerically erroneous peak.

Figure 7 shows the fully Coriolis-coupled reaction probabilities for the HD_2^- system, which can be compared with those for the H_3^- system (Figure 8); for CPU reasons, we limited ourselves to coupling up to $\Omega_{max} = 8$ (see eqs 6 and 18). We

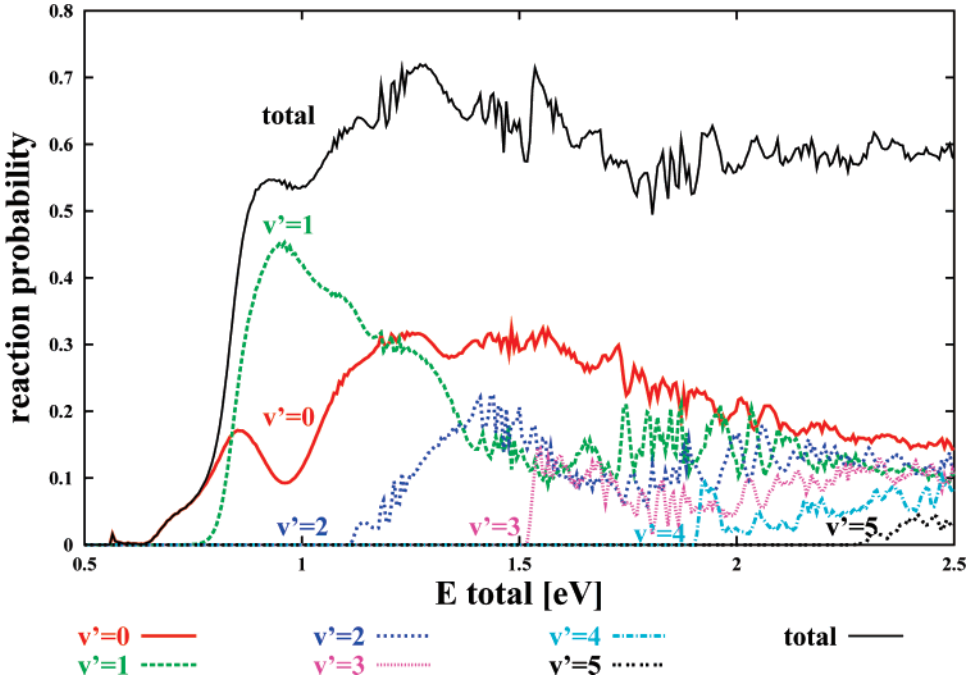

Figure 4. $H^- + D_2(v = 1, j = 0)$. State-to-state reaction probabilities (summed over rotational states) with $J = 0$, $R_{max} = 17.5a_0$, $E_{trans}^{WP} = 1$ eV.

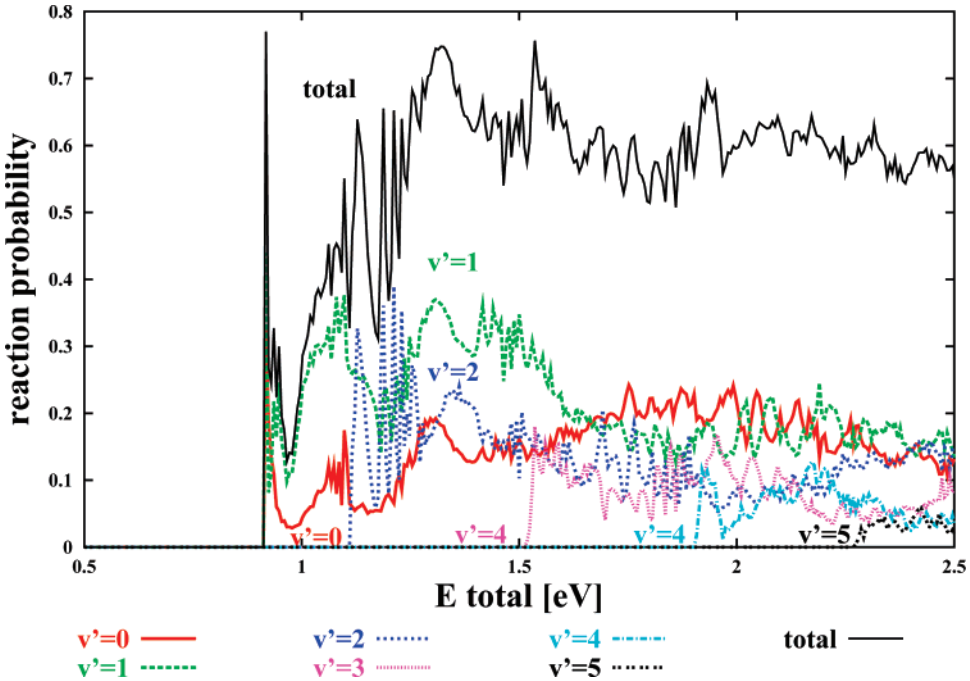

Figure 5. $H^- + D_2(v = 2, j = 0)$. State-to-state reaction probabilities (summed over rotational states) with $J = 0$, $R_{max} = 17.5a_0$, $E_{trans}^{WP} = 1$ eV.

calculated the J-dependence of $P_{reac}(E)$ to get information about the integral reactive cross section $\sigma^{tot}(E)$ (for initial quantum numbers v, j) (as presented in Figure 9),

$$\sigma^{tot}(E) = \frac{\pi}{k_{vj}^2}\sum_J (2J+1)P_{reac}^J(E) \qquad (19)$$

a property directly comparable with experiment. Calculations for differential cross sections and partial cross sections ($\sigma_{v'}$) are in progress and should reveal clearly the quality of the potential energy surface. For the moment we have to rely on integral cross sections ($\sigma^{tot} = \sum_{v'}\sigma_{v'}$). As one can see from Figure 9 (HD_2^-), the overall behavior of the different theoretical results fits well with the guided-beam measurements of Haufler et al.[13] and the crossed-beam measurements of Zimmer and Linder.[12] In the experimental setups, the initial conditions for the D_2 molecule were not assigned to the ideal quantum numbers $v = 0$ and $j = 0$; in the work of Zimmer and Linder, all target molecules can be assumed to be in the vibrational ground state $v = 0$ with a population of the rotational levels of n-D_2 at an estimated gas beam temperature of $T_{rot} = 180$ K: $j = 0$ (29.9%), $j = 1$ (27.5%), $j = 2$ (34.7 %), $j = 3$ (5.7%), $j \geq 4$ (2.2%). In the guided-beam measurements,[13] the rovibrational states for D_2 are thermally averaged as a result of a gas temperature of $T = 300$ K; i.e., a few low vibrational states and not only low rotational states are present during the collision experiment. The error bars in the work of Zimmer and Linder[12] are indicated in Figure 9 and are relatively large, at least in the energy range

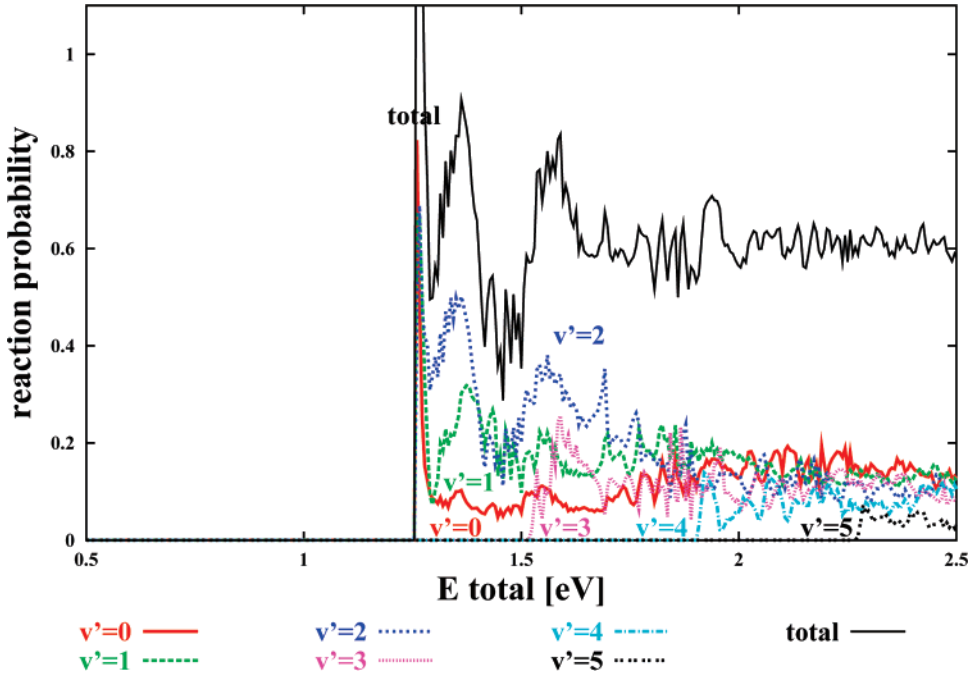

Figure 6. $H^- + D_2(v = 3, j = 0)$. State-to-state reaction probabilities (summed over rotational states) with $J = 0$, $R_{max} = 17.5a_0$, $E_{trans}^{WP} = 1$ eV.

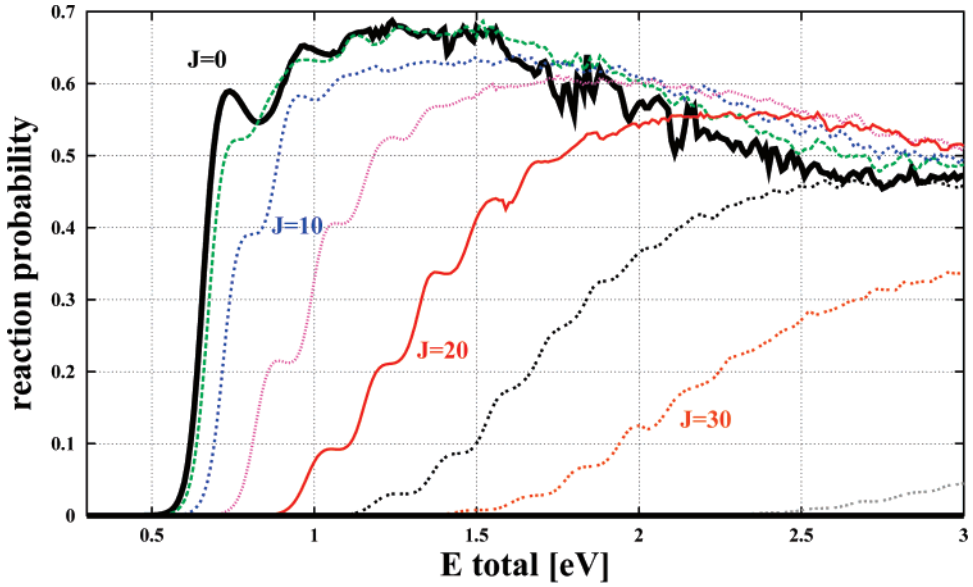

Figure 7. $H^- + D_2(v = 0, j = 0)$. Total reaction probabilities (complex wave packets, SM potential) for different values of $J = 0$, 5, 10, 15, 20, 25, 30, 40 ($\Omega_{max} = 8$) using reactant coordinates (RC) (grid(R,r,θ) = 128,64,32; $R_{max} = 17.5a_0$, $E_{trans}^{WP} = 1$ eV).

1−2 eV, and hide the oscillatory structure of the data. The error bars of Haufler et al.[13] are smaller but account only for statistical uncertainty, as claimed by the authors. There is a deviation at the onset of the reaction where the values of Zimmer and Linder[12] agree better with theory than the one of Haufler et al.[13] The results of Huq et al.,[36] where D^- reaction products and inelastically scattered H^- were detected likewise (i.e., no mass separation was available), can serve as an upper limit only.

Integral cross sections are often empirically estimated by using the J-shift approach of Bowman[39−41] with data from, e.g., $J = 0$ results ($P_{reac}^J(E) = P_{reac}^{J=0}(E - E_{shift})$). The method relies on the identification of a "bottleneck", such as a transition state. The changes in the rotational energy (i.e., changing J) of the system, when fixed at the geometry of the barrier position (i.e., transition state R_{TST}), provide an energy shift E_{shift}. This estimation might be justified for cases with a relatively simple, activated process, like the H_3^- system. We estimated $R_{TST} = 3.5a_0$ for the rotational energy $E_{TST}^{rot} = E_{shift} = J(J + 1)/2\mu_R R_{TST}^2$ by trying to reproduce the correct onset of the Coriolis-coupled results (i.e., this has been tested in comparison with accurate calculation for $J = 5$ and 10). Because J-shifting cannot estimate the change of magnitude of the individual P_{reac}^J contributions, i.e., in the present case the decrease of P_{reac}^J (see Figure 7), it is of minor importance for the present reaction when comparing with experimental results.

The "best" theoretical results ("with Coriolis coupling" in Figure 9) include the summation of reaction probabilities P_{reac}^J calculated for individual J values (up to $J = 60$). In Figure 7, explicitly calculated P_{reac}^J values for up to $J = 40$ (with $\Omega_{max} = 8$) had been presented; P_{reac}^J values for $J = 21-24$, 26−29, 31−39, 41−49 had been calculated by linear interpolation. The contribution of $J = 50$ is negligible at energies $E < 2.5$ eV. For a further assessment of the comparison of experiment and

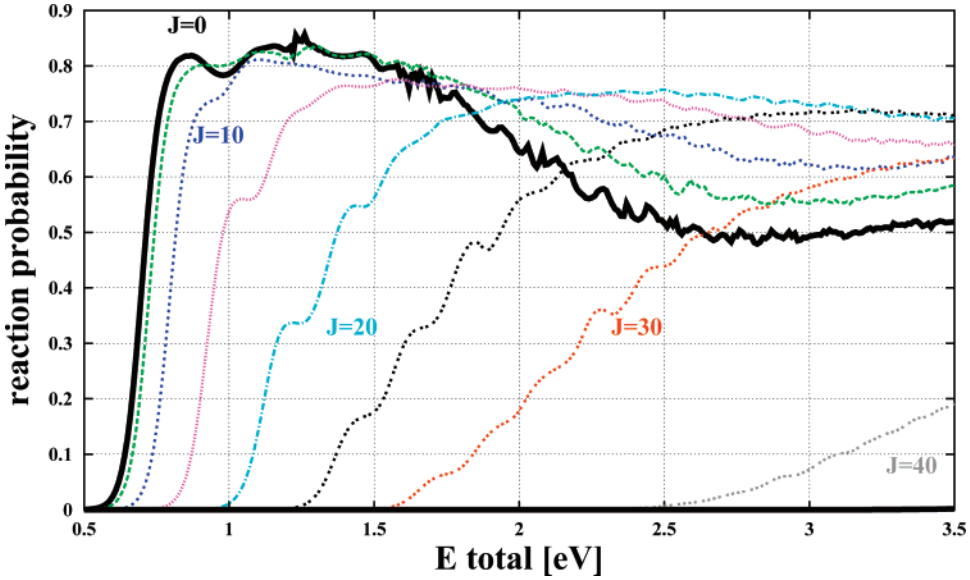

Figure 8. $H^- + H_2(v = 0, j = 0)$. Total reaction probabilities (complex wave packets, SM potential) for different values of $J = 0$, 5, 10, 15, 20, 25, 30, 40 ($\Omega_{max} = 8$) using reactant coordinates (RC) (grid(R,r,θ) = 128,64,32; $R_{max} = 17.5a_0$, $E^{WP}_{trans} = 1$ eV).

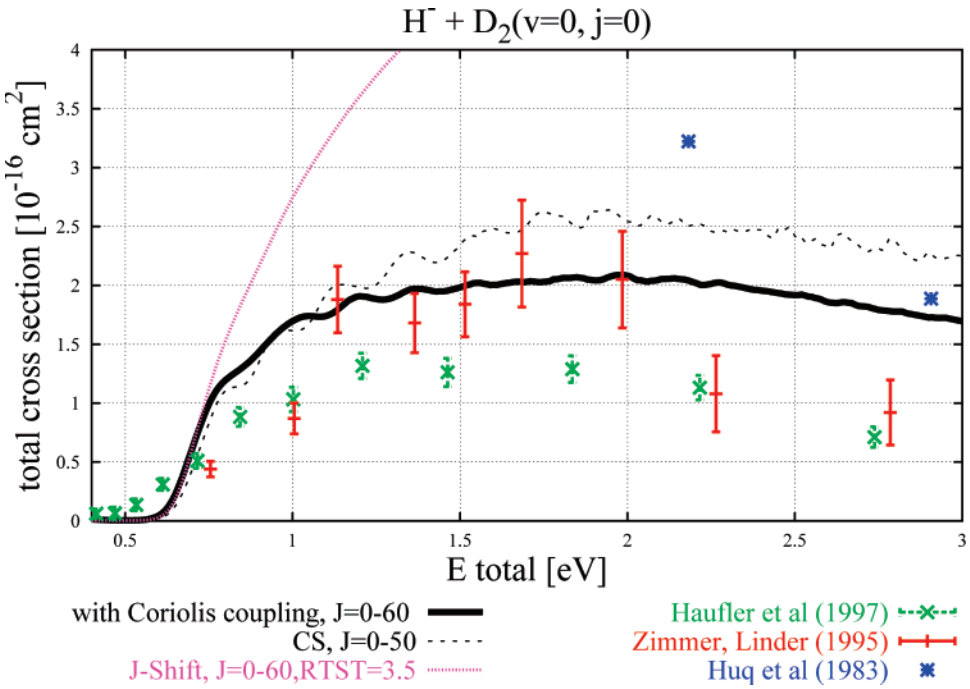

Figure 9. Cross sections for $H^- + D_2(v = 0, j = 0)$. Cross sections based on fully Coriolis-coupled calculations and the centrifugal sudden approximation (CSA) ($J = 0-50$) are compared with empirical J-shift calculations ($R_{TST} = 3.5a_0$; correct increase at the onset) and experimental results of Zimmer and Linder[12] (crossed beam, $D_2(v = 0$, low j's)), Haufler et al.[13] (D_2, 300 K, thermally averaged rovibrational states), and Huq et al.[36] (can serve as an upper limit only).

theory, we included the cross sections resulting from a centrifugal sudden approximation (CSA) treatment of the dynamics, i.e., no Coriolis coupling: calculations only for $\Omega = 0$ and initial $j = 0$. The $P^{(CS)J}_{reac}(E)$ (not shown here explicitly) values do oscillate even at higher J values (similar to $P^{J=0}_{reac}(E)$ in Figure 7) and level off much slower with increasing J compared to the curves given in Figure 7. This results in much larger cross sections, which still shows oscillatory structure. Each individual P^J_{reac} contribution to the total cross section is presumably numerically correct up to $E \approx 3$ eV. Limiting ourselves to $\Omega_{max} = 8$ probably has a minor influence on the cross section. In the case of $J = 15$, we compared the results for $\Omega_{max} = 8$ and $\Omega_{max} = 15$: the general shape and magnitude of $P^{J=15}_{reac}(E)$ had not changed dramatically. The results for the cross sections can be slightly influenced by the too small size of the interaction region and choice of the cutoff parameters (see eqs 9, 10, and 12 for ΔE, E_{max}, and E_{min}). Furthermore, deviations between theory and experiment might be due to inadequacies in the potential energy surface. But, as already discussed, for energies larger than 1.2 eV, the coupling to higher electronically excited states (i.e., ionization to $HD_2(H_3)$ plus one free electron) has to be included in the dynamics. This influence is hard to estimate, but it would explain why experimentally a decrease in the cross section is already noticed before 2 eV. Further deviations from experiment rely on the comparison of different initial conditions between calculations ($D_2(v = 0, j = 0)$) and experiment (at least several low-lying rotational states are populated). Preliminary calculations for rotationally excited

states of D_2 and for $J > 0$ indicate that the oscillatory structure in the experimental cross sections of Zimmer and Linder[12] result from contributions of $D_2(j > 0)$.

4. Summary

For the dynamics of reactive scattering processes of ion−neutral reactions $H^- + D_2$ and $H^- + H_2$, time-dependent wave packet calculations have been performed. The ab initio potentials used in the present calculations exhibit long-range interactions, which leads to CPU-intensive calculations. The energy-resolved and state-to-state analysis had been performed in reactant and/or product Jacobi coordinates.

Earlier work has shown that the Chebychev method is a numerically efficient technique for solving wave packet (WP) propagation, especially when using the code on multiprocessor machines; the accuracy can be consecutively improved by propagating in time as long as it is needed. The recursion formula in eq 10 is independent of the magnitude of the time step. The efficiency of the wave packet approach compared to the time-independent hyperspherical approach of Manolopoulos et al.[37] is such that, in case a fine energy grid for the reaction probability was needed, the time-independent approach was more time-consuming. WPs are relatively easy to apply for systems with many reaction channels and are suitable for use on several PESs, and with WPs one gets with one calculation information about a large collision energy range ($\Delta E_{coll} \approx 4$ eV). The disadvantage is that, in case of deep potential energy minima, WP calculations can become very CPU-intensive, because the wave packet is trapped.

In the case of the HD_2^- system, we present energy-resolved and state-to-state reaction probabilities for different starting conditions, i.e. different rovibrational states of the reactant molecule D_2. It is the first time that the nuclear dynamics within this system has been investigated in such a detail using the ab initio potential of Stärck and Meyer.[10] For a few exemplary test cases ($J = 0$) we found quantitative agreement with the "real wave packet" code of Gray[42] and with the "abc" code (time-independent hyperspherical coordinate method) of Manolopoulos et al.[37]

The computed cross sections $\sigma(E)$ are in good agreement with experimental results for energies below the opening of the electron detachment channel ($E \approx 1.2$ eV). At higher energies ($E > 2.0$ eV), theory overestimates $\sigma(E)$. A better direct comparison between theory and experiment can be made when the population of the different initial rovibrational states in the experiment has been taken into account and when numerical, fully converged partial integral and differential cross sections are available.

Acknowledgment. The authors thank S. Gray for support and discussions. This work was supported in part by the Deutsche Forschungsgemeinschaft within the former Schwerpunktprogramm "Zeitabhängige Phänomene und Methoden in Physik und Chemie". The computations were performed on the Compaq ES20 and AMD-64-Opteron Cluster of the Computercenter in Siegen (HRZ) and on the IBM-SP2 at the Computercenter of the University of Karlsruhe (SSC). We thank SSC and HRZ for computer time.

References and Notes

(1) Althorpe, S. C.; Clary, D. C. *Annu. Rev. Phys. Chem.* **2003**, *54*, 493.
(2) Jaquet, R.; Heinen, M. *J. Phys. Chem. A* **2001**, *105*, 2738.
(3) Baer, M., Ng, C. Y., Eds. *State-Selected and State-to-State Ion−Molecule Reaction Dynamics: Experiment and Theory*; Advances in Chemical Physics 81 and 82; Wiley: New York, 1992.
(4) Morari, C.; Röhse, R.; Jaquet, R. In *High Performance Computing in Science and Engineering 2000*; Krause, E., Jäger, W., Eds.; Springer: Berlin, 2001; p 207.
(5) Cencek, W.; Rychlewski, J.; Jaquet, R.; Kutzelnigg, W. *J. Chem. Phys.* **1998**, *108*, 2831; 2837.
(6) Röhse, R.; Kutzelnigg, W.; Jaquet, R.; Klopper, W. *J. Chem. Phys.* **1994**, *101*, 2231.
(7) Jaquet, R. *Spectrochim. Acta A* **2002**, *58*, 691.
(8) Pendergast, P.; Heck, J. M.; Hayes, E. F.; Jaquet, R. *J. Chem. Phys.* **1993**, *98*, 4543.
(9) Jaquet, R. *Theor. Chim. Acta* **1994**, *88*, 217.
(10) Stärck, J.; Meyer, W. *Chem. Phys.* **1993**, *176*, 83.
(11) Belyaev, A. K.; Colbert, D. T.; Groenenboom, G. C.; Miller, W. H. *Chem. Phys. Lett.* **1993**, *209*, 309.
(12) Zimmer, M.; Linder, F. *J. Phys. B: At. Mol. Opt. Phys.* **1995**, *28*, 2671.
(13) Haufler, E.; Schlemmer, S.; Gerlich, D. *J. Phys. Chem. A* **1997**, *101*, 6441.
(14) Kosloff, R. *J. Phys. Chem.* **1988**, *92*, 2087.
(15) Tal-Ezer, H.; Kosloff, R. *J. Chem. Phys.* **1984**, *81*, 3967.
(16) Mandelshtam, V.; Taylor, H. S. *J. Chem. Phys.* **1995**, *103*, 2903.
(17) Heather, R.; Metiu, H. *J. Chem. Phys.* **1987**, *86*, 5009.
(18) Neuhauser, D.; Baer, M.; Hudson, R. S.; Kouri, D. J. *Comput. Phys. Commun.* **1991**, *63*, 460.
(19) Leforestier, C. *J. Chem. Phys.* **1991**, *94*, 6388.
(20) Balint-Kurti, G. G.; Dixon, R. N.; Marston, C. C. *Int. Rev. Phys. Chem.* **1992**, *11*, 317.
(21) Brigham, E. O. *The Fast Fourier Transformation: An Introduction to its Theory and Application*; Prentice Hall: Englewood Cliffs, NJ, 1974.
(22) Light, J. C.; Hamilton, I. P.; Lill, J. V. *J. Chem. Phys.* **1985**, *82*, 1400.
(23) Gray, S. K.; Balint-Kurti, G. G. *J. Chem. Phys.* **1998**, *108*, 950.
(24) Vibok, A.; Balint-Kurti, G. G. *J. Phys. Chem.* **1992**, *96*, 8712.
(25) Goldfield, E. M.; Gray, S. K. *Comput. Phys. Commun.* **1996**, *98*, 1.
(26) Zhu, W.; Peng, T.; Zhang, J. Z. H. *J. Chem. Phys.* **1997**, *106*, 1742. Peng, T.; Zhang, J. Z. H. *J. Chem. Phys.* **1996**, *106*, 6072.
(27) Kouri, D. J.; Hoffman, D. K.; Peng, T.; Zhang, J. Z. H. *Chem. Phys. Lett.* **1996**, *262*, 519.
(28) Althorpe, S. C.; Kouri, D. J.; Hoffman, D. K. *J. Chem. Phys.* **1997**, *107*, 7816; *J. Phys. Chem. A* **1998**, *102*, 9494.
(29) Althorpe, S. C. *Faraday Discuss.* **1999**, *110*, 238.
(30) Althorpe, S. C. *J. Chem. Phys.* **2001**, *114* 1601.
(31) Meijer, A. J. H. M.; Goldfield, E. M.; Gray, S. K.; Balint-Kurti, G. G. *Chem. Phys. Lett.* **1998**, *293*, 270.
(32) Aguillon, F.; Belyaev, A. K.; Sidis, V.; Sizun, M. *Phys. Chem. Chem. Phys.* **2000**, *2*, 3577.
(33) Gianturco, F. A.; Kumar, S. *J. Phys. B: At. Mol. Opt. Phys.* **1997**, *30*, 3031.
(34) Mahapatra, S.; Sathyamurthy, N. *Faraday Discuss.* **1998**, *110*, 228.
(35) Mahapatra, S. *Phys. Chem. Chem. Phys.* **2000**, *2*, 671.
(36) Huq, M. S.; Doverspike, L. D.; Champion, R. L. *Phys. Rev. A* **1982**, *27*, 2831.
(37) Skouteris, D.; Castillo J. F.; Manolopoulos, D. E. ABC: The CCP6 Quantum Reactive Scattering Program. *Comput. Phys. Commun.* **2000**, *133*, 128.
(38) Panda, A. N. Ph.D. work, ITT Kanpur, India, 2004 (unpublished).
(39) Bowman, J. M. *Adv. Chem. Phys.* **1985**, *61*, 115.
(40) Bowman, J. M. *J. Phys. Chem.* **1991**, *95*, 4960.
(41) Sun, Q.; Bowman, J. M.; Schatz, G. C.; Connor, J. N. *L. J. Chem. Phys.* **1990**, *92*, 1677.
(42) Gray, S. K., "real wavepacket" code.[23]